Bulletin of Mathematical Biology (2001) **63**, 1125–1161
doi:10.1006/bulm.2001.0262
Available online at http://www.idealibrary.com on IDEAL®

Two-category Model of Task Allocation with Application to Ant Societies

WENDY A. M. BRANDTS AND ANDRÉ LONGTIN*
Department of Physics,
University of Ottawa,
150 Louis Pasteur,
Ottawa, Ont.,
Canada K1N 6N5

LYNN E. H. TRAINOR
Department of Physics,
University of Toronto,
Toronto, Ont.,
Canada

In many network models of interacting units such as cells or insects, the coupling coefficients between units are independent of the state of the units. Here we analyze the temporal behavior of units that can switch between two 'category' states according to rules that involve *category-dependent coupling coefficients*. The behaviors of the category populations resulting from the asynchronous random updating of units are first classified according to the signs of the coupling coefficients using numerical simulations. They range from isolated fixed points to lines of fixed points and stochastic attractors. These behaviors are then explained analytically using iterated function systems and birth–death jump processes. The main inspiration for our work comes from studies of non-hierarchical task allocation in, e.g., harvester ant colonies where temporal fluctuations in the numbers of ants engaged in various tasks occur as circumstances require and depend on interactions between ants. We identify interaction types that produce quick recovery from perturbations to an asymptotic behavior whose characteristics are function of the coupling coefficients between ants as well as between ants and their environment. We also compute analytically the probability density of the population numbers, and show that perturbations in our model decay twice as fast as in a model with random switching dynamics. A subset of the interaction types between ants yields intrinsic stochastic asymptotic behaviors which could account for some of the experimentally observed fluctuations. Such noisy trajectories are shown to be random walks with state-dependent biases in the 'category population' phase space. With an external stimulus, the parameters of the category-switching rules become time-dependent. Depending on the growth rate of the stimulus in comparison to its population-dependent decay rate, the dynamics may qualitatively differ from

*Author to whom correspondence should be addressed. *E-mail*: alongtin@physics.uottawa.ca

0092-8240/01/061125 + 37 $35.00/0

the case without stimulus. Our simple two-category model provides a framework for understanding the rich variety of behaviors in network dynamics with state-dependent coupling coefficients, and especially in task allocation processes with many tasks.

1. INTRODUCTION

1.1. ***Non-hierarchical task allocation.*** Task allocation is a process that directs individuals or units into particular categories or modes of behaviors (tasks), without centralized control. Instead, simple local information exchanged between units or between a unit and its environment allows the system to beneficially regulate the number of individuals carrying out various tasks and properly respond to environmental changes (Gordon, 1996). Models of task allocation aim to determine the extent to which *interactions* between essentially identical individuals, rather than intrinsic differences between individuals, account for group behavior. Examples of task allocation in biology include division of labor in insect societies (Gordon *et al.*, 1992; Tofts and Franks, 1992; Deneubourg and Franks, 1995; Bonabeau *et al.*, 1997, 1998a), gene regulation and transcription (Somogyi and Sniegoski, 1996), and cellular differentiation. Applications beyond insect societies include human job markets and group dynamics (Trainor *et al.*, 1993, 1997), and general studies of the interaction between task diversity and the specialization of individuals in communities [see, e.g., Borkar *et al.* (1998)].

In certain insect societies, division of labor is a function of specific physical attributes of the individuals such as size. However, bees, wasps and most ant species are monomorphic (i.e., there is only one size of worker), and polymorphism can thus not account for task allocation (Gordon, 1996). It is known that in many monomorphic insect colonies, the number of workers performing a given task is adjusted according to the changing needs of the colony. In fact, in species such as harvester ants, the numbers of workers engaged in each task continually change, even hour to hour (Gordon, 1999a). Further, tasks in those colonies are interdependent, meaning that the number of workers that go into each specific task is a function of the number of workers currently performing each task.

Our work ultimately concerns the emergence of such non-hierarchical task allocation through interactions between individuals, with and without a global environmental stimulus. However, the study of the dynamics of a collection of interacting units such as cells or agents poses great challenges (Parrish and Edelstein-Keshet, 1999; Beshers and Fewell, 2001). Models which are complex enough to exhibit a range of interesting dynamical behaviors are usually too complex to characterize fully either analytically or numerically. Often the analysis of such systems eludes treatment because of the combination of deterministic and stochastic dynamics, as well as the possible coexistence of many attractors for a given parameter set,

i.e., 'multistability' (Poon and Grebogi, 1995). These problems have received considerable attention in the context of neural networks. For example, the Hopfield model (Hopfield, 1982) of a network of globally coupled neurons with symmetric interactions is an exceptional example of a system where the dynamical behaviors, and the multistability in particular, are well-understood owing to the existence of a global Lyapunov function.

There are numerous examples of other networks, neural, genetic, immunological, societal and other where the dynamics are not so well understood, either because the couplings are asymmetric, time- or state-dependent, or simply because units can have more than two states. Much progress has nevertheless been made. For example, the complex dynamics of neural networks have been studied using spin-glass theory (Hertz *et al.*, 1991) and symbolic dynamics on N-dimensional hypercubes (Lewis and Glass, 1992). Studies of collective computations in societies, induced by interactions among individuals, have made use of globally coupled maps and statistical complexity theory [see, e.g., Delgado and Solé (1998) and references therein]. And our knowledge of genetic and evolutionary networks has been advanced through the analysis of Boolean networks (Kauffman, 1990) and special classes of differential equations (Hofbauer and Sigmund, 1991). One result of our paper is that stochastic processes known as birth–death jump processes with state-dependent transition probabilities are useful for studying nonhierarchical task allocation.

1.2. ***State-dependent coupling strengths and task allocation.*** Interactions between units depend on coupling strengths, which are typically assumed constant unless, as in training a neural net, the system is in a learning mode. For example, for 'classical' neural networks, the rule that governs the switching between neuron states uses a weighted sum over the (analog or digital) states of other neurons (Hertz *et al.*, 1991), and the coupling strength between two neurons does not depend on the state of these neurons. Likewise, in the Ising model of magnetic spins (which has much inspired the neural network literature), the contribution to the energy function of each pairwise interaction involves the triple product of each state in a pair and a coupling coefficient. This coefficient does not depend on the states (up or down) of the spins in the pair, but rather on the physics (e.g., ferromagnetic vs anti-ferromagnetic) of the magnetic interaction.

The specific focus of our paper is the dynamical behavior of a population of units whose coupling coefficients depend on the 'state' of those units. Task allocation has recently been modeled using this state-dependent coefficient approach (Gordon *et al.*, 1992). The model ants in that study change categories through deterministic switching rules based on fields, which can be interpreted as the summed chemical or contact cues from other individuals. Conditions were found for which the time evolution of category populations showed similarities to experimental data on task allocation in certain ant species. Numerical analysis of the model also revealed a fascinating and bewildering array of dynamical behaviors including multista-

bility, a consequence of the large number (eight) of categories assumed in their model.

1.3. ***From eight to two categories.*** The complexity of the eight-category model of Gordon *et al.* (1992), with its three fields and numerous parameters, has severely impeded efforts to organize the dynamical behaviors of this class of models and to gain strong intuition about its properties, though some progress has been made (Torres and Trainor, 1993; Trainor *et al.*, 1997). Consequently, it is difficult to constrain model parameters, such as the numerous interaction coefficients, using experimental data. The problem would be larger still if environmental effects, such as the circadian activity of the nest, or population age-structure properties such as temporal polyethism, were to be accounted for.

There is, nevertheless, a need to better understand task allocation dynamics arising from explicit interactions between units performing different tasks [see Section 2.1, Gordon (1999a), and Bonabeau *et al.* (1998a)]. This fact, together with the aforementioned problems with the eight-category model, inspires the analysis of the two-category model presented in this paper. Its architecture is simple enough to allow us to determine analytically its surprisingly rich repertoire of dynamical behaviors. And in the presence of an external stimulus (such as the availability of food), our analysis also allows us to understand some of the very wide range of behaviors. Our goal is achieved through numerical simulation, as well as analytical work that reduces the dynamical behavior to that of an iterated function system and also of a birth–death stochastic process. All possible interaction matrices are classified into a limited number of category interaction types, which in turn determine the resulting attractors and their basins. Our analysis provides much needed insight into the nature of the solutions and complexity of many-category models. It reveals the types of category interactions that lead to stable populations that recover quickly from perturbations, and that allow the 'equilibrium' populations to be chosen by suitable parameter choices.

In Section 2, we describe the two-category model and its switching rules, and analyze the intrinsic dynamics (i.e., without external stimuli) in terms of analytically determined critical population numbers. In Section 3, we classify the key behaviors of the model using the concepts of attractors and of activation/inhibition. We also characterize the decay time of perturbations from the attractors, and further compare these features to those for random switching dynamics. Section 3 ends with a summary of couplings that produce attractors. In Section 4, we present another dynamical view of our two-category model, based on two discrete-time maps that are used with varying probability at each time step. This 'iterated function system' in turn suggests a birth–death stochastic process formulation. Solving the associated master equation (Appendix A) yields the exact steady-state probability distribution of population numbers. The task allocation process is then explained intuitively as a random walk in a quadratic potential between reflecting boundaries, themselves computable functions of the interaction matrix coefficients. Section 5

gives a preliminary analysis of the range of behaviors to be expected when the units interact not only between themselves, but also with an external stimulus that can be altered by the units (such as a food source). The discussion and outlook onto future work follow in Section 6.

2. TWO-CATEGORY NETWORK MODEL

2.1. ***Background for modeling task allocation.*** Models of task performance and task allocation in insect societies have focused on interactions between units, and between units and their environments [see, e.g., the different kinds of foraging organization in ant species in Deneubourg *et al.* (1986)]. An excellent review of modeling studies of task allocation in the context of ant societies can be found in Bonabeau *et al.* (1998a) and Beshers and Fewell (2001). Recent work has shown how regulation of tasks can arise from decisions based on exposure to stimuli, without any explicit interaction between individuals [see the threshold model of Bonabeau *et al.* (1998a), or the foraging for work model of Tofts and Franks (1992)]. Interestingly, Bonabeau *et al.* noted, despite the success of their model, that as ants probably update their tasks by also using information from direct interactions with other ants, a full model should combine both kinds of interactions. Earlier, Page and Mitchell (1990) proposed a Boolean network model of task allocation in honey bees in which a binary unit (a bee) switches state based on the sum of contributions from the units it is connected to, as well as on external fields (related to task-specific stimuli). Our model, like the threshold network model of Gordon *et al.* (1992), which is its inspiration, shares some similarities with that of Page and Mitchell, except that it focuses on the emergence of task regulation through interaction between units, and its coupling coefficients change with the states of the units. Our work is thus complementary to this and other threshold models.

Specifically, our model involves a collection of identical units which belong to either of two categories. Even though they are in principle identical, units can take on different tasks based on the stimuli they have received from other units. In the case of ants, these stimuli are probably communicated through antenna contacts, trophallaxis (exchange of food), or pheromone fields. One possible assignment of the two categories is the total populations of active vs inactive ants in, e.g., the Gordon *et al.* (1992) or Solé *et al.* (1993) models. This latter work [see also Delgado and Solé (1998)] analyzes short-term oscillations in the number of active ants in a certain species, with state-dependent coupling coefficients as in Gordon *et al.* (1992). In contrast with our work, their analysis relies on Markov chains, is confined to a coupling matrix with positive identical elements, and focuses on the critical density of ants necessary for oscillations to appear; ants also become spontaneously active with a certain probability in their model.

An alternate possible assignment of the two categories is to the populations inside vs outside the nest (Sendova-Franks and Franks, 1995). The number of ants that a

given ant surveys to update its task is a parameter in our model. This number will be dependent on the particular modeling context, e.g., on the ant species, on how well the populations are mixed (such as near the entrance of the nest), or on the specific properties (local vs global, persistence) of the cues used for updating.

Our model aims to capture the fashion in which a population can be organized or subdivided into categories dynamically so that the category any unit finds itself in stays fixed changes from time to time; and overall, category populations are maintained within some range of values. Thus we want stable population numbers and a stable and rapid 'regulatory' response to perturbations. Additionally, we wish to understand how these properties depend on the state-dependent coupling strengths between units, as well as on the parameters underlying the interaction of the units with external stimuli (such as food sources) (Section 5). We will assume that interactions may be asymmetric and that units are updated asynchronously. Finally, our model should ideally be flexible enough to allow arbitrary values for both the stable category populations (attractor location) and their range of variation (attractor width). The important variables are the category populations, which are experimentally accessible observables.

2.2. ***Category switching rules: field thresholds.*** In the two-category model examined here, each unit i in a set of N identical units is characterized by a binary variable S_i. All units with $S_i = 1$ are defined to be in category 1, and those with $S_i = -1$ in category 2. The fundamental interaction between the ith and jth units is category dependent. Since there are only two categories, there are four matrix elements,

$$\alpha_{IJ} = \begin{pmatrix} \alpha_{11} & \alpha_{12} \\ \alpha_{21} & \alpha_{22} \end{pmatrix},$$

where α_{ij} corresponds to the effect on a unit in category i of a unit in category j. The two-category model was first proposed and briefly analyzed numerically in Trainor *et al.* (1997), using a switching rule that ensured the monotonic decrease of an energy function (a 'spin-alignment' rule), and a symmetric interaction matrix. Here, we consider switching rules based on the values of fields with respect to thresholds, and do not impose any symmetry on the interaction matrices. We then explore the whole range of possible dynamics for this model.

The variables of interest are n_1 and n_2, the population in category 1 and 2, respectively, with $n_1 + n_2 = N$. Dynamics are generated by the *switching rules*, which determine whether a unit, chosen at random for updating, will switch categories. We associate with each unit i a field F_i, which is a weighted sum of inputs from all other elements excluding the interaction of a unit with itself, viz.

$$F_i = \sum_{k=1}^{2} n_k \alpha_{ik} S_k - \alpha_{ii} S_i,$$

where k runs over categories (1 and 2). The second term on the right-hand side cancels out the interaction of unit i with itself which has been included in the sum. Note that we will distinguish this interaction of a unit with itself from what we will call 'self-interaction', by which we designate the interaction of a unit with another unit *in the same category*. Also, we have assumed that the unit computes its field over the whole population. The effect of computing the field over a fraction of the population on the dynamics will be discussed in Section 6.

The switching rules are taken as follows. A unit in category 1 will switch to category 2 upon updating if $F_1 < 0$. Likewise, a unit in category 2 will switch to category 1 if $F_2 > 0$. In numerical simulations we used an asynchronous updating procedure wherein a unit was chosen at random for updating, its field evaluated, the switching rule applied, and then the category updated. The dynamics of the switching rule are entirely deterministic but stochasticity enters in the choice of unit that will be updated.

Despite this stochastic element, important characteristics of the dynamics as a function of the category interaction matrix elements can be derived. For a given α_{IJ} we can determine *critical population* values n_a and n_b (defined later), above or below which switching can occur. *These critical population values define the boundaries of dynamical structures in the model.* Looking again at our expression for the field, we find that for a unit in category 1, the field F_1 can be expressed as:

$$F_1 = n_1\alpha_{11}S_1 + n_2\alpha_{12}S_2 - \alpha_{11}S_1 \tag{1}$$

$$= n_1(\alpha_{11} + \alpha_{12}) - \alpha_{11} - N\alpha_{12}. \tag{2}$$

For a unit in category 2, the field F_2 is:

$$F_2 = n_1\alpha_{21}S_1 + n_2\alpha_{22}S_2 - \alpha_{22}S_2 \tag{3}$$

$$= n_1(\alpha_{21} + \alpha_{22}) - (N-1)\alpha_{22}. \tag{4}$$

According to the switching rules, when a unit in category 1 is chosen for updating, it will switch categories if $F_1 < 0$, that is, if

$$n_1(\alpha_{11} + \alpha_{12}) < \alpha_{11} + N\alpha_{12}.$$

Similarily, a unit in category 2 will switch if $F_2 > 0$, that is, if

$$n_1(\alpha_{21} + \alpha_{22}) > (N-1)\alpha_{22}.$$

We define critical population values as:

$$n_a = \frac{\alpha_{11} + N\alpha_{12}}{\alpha_{11} + \alpha_{12}}, \qquad n_b = \frac{(N-1)\alpha_{22}}{\alpha_{22} + \alpha_{21}}.$$

The result of applying the switching rules is thus that a unit in category 1 will switch if

1. $n_1 < n_a$, for $(\alpha_{11} + \alpha_{12}) > 0$, or if
2. $n_1 > n_a$, for $(\alpha_{11} + \alpha_{12}) < 0$.

Similarly, a unit in category 2 will switch if

1. $n_1 > n_b$, for $(\alpha_{22} + \alpha_{21}) > 0$, or if
2. $n_1 < n_b$, for $(\alpha_{22} + \alpha_{21}) < 0$.

Furthermore, since $0 \leq n_1 \leq N$, we can determine the outcome of the switching dynamics as a function of particular signs and magnitudes of the interaction matrix. This follows because n_a and n_b can be calculated once the α matrix is known.

3. MODEL DYNAMICAL BEHAVIORS

3.1. ***Characterizing behaviors.*** In this section, we examine the range of characteristic behaviors which arise from different choices of the elements of the interaction matrix, and in particular, their sign patterns. The inclusion of coupling to an environmental stimulus that can be altered by the units (such as a food source depleted by foraging ants) will be studied later in Section 5. It will prove useful to classify the matrix elements of interaction pairs in terms of their effects with respect to *activation* and *inhibition*. It will also prove useful to draw on concepts from dynamical systems theory.

Because the spatial position of units is not considered in our two-category model, the only state variables of interest are the discrete variables n_1 and n_2. Further, since $N = n_1 + n_2$, there is only one independent state variable, which we will choose as n_1. A spatial extension of our model onto a spatial lattice would be straightforward.

An *attractor* is a region of population space that is invariant under the dynamics, i.e., a set of points that transforms into itself as time evolves, and that attracts neighboring points; together these neighbors and the attractor form the *basin of attraction*. A *repeller* is an invariant set which cannot be reached from outside. The attractors and repellers in our study can further be characterized as *deterministic*, having a strictly predictable constant value, or *stochastic*, where fluctuations occur within their boundaries. The deterministic attractor/repeller consists here of one or more contiguous population values, each of which is a fixed point. The extent of a stochastic attractor includes every point that can be reached through fluctuations.

Figure 1 illustrates the coexistence of a line of fixed points and a stochastic attractor; note that the fluctuations in this attractor are always on the lower side of $n_b = 16.5$. A line of fixed points may more appropriately be called 'interval of fixed points in the discrete phase space $(0, N)$', but we will nevertheless use the more common terminology 'line of fixed points'. With two categories, we find from our numerical simulations that there exist at most two attractors or repellers. Dynamical evolution can either be constant, change monotonically with fluctuations, or just fluctuate randomly.

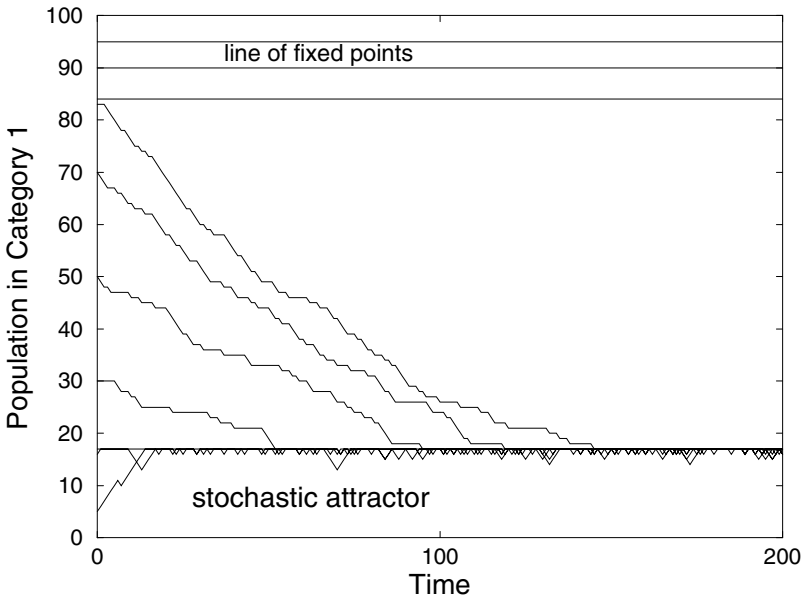

Figure 1. Category 1 population vs time for various initial conditions from model simulations of an activator–inhibitor interaction. The system exhibits bounded fluctuations on a stochastic attractor for $n_1 < n_b$, monotonically decaying solutions for $n_b < n_1 < n_a$ that lead to the trapping region $n_1 < n_b$, and constant solutions for the line of fixed points $n_a < n_1 < N$. $N = 100$, $\alpha_{11} = 1$, $\alpha_{12} = 5$, $\alpha_{21} = -5$, $\alpha_{22} = -1$. Here $n_a = 83.5$ and $n_b = 16.5$.

3.2. ***Activators, inhibitors, bigots and loners.*** The units of each category will be classified according to whether their self-interaction (i.e., their interaction with other units in the same category) is activating or inhibiting, and whether their effect on the other category of units is activating or inhibiting (see Table 1, and the following text). From the switching rules, it is clear that a positive α_{11} and a negative α_{12} have an activating effect on category 1, in the sense of increasing or stabilizing its population. Similarly, for a unit in category 2, a negative α_{21} and a positive α_{22} have an activating effect on population n_2. The activator–activator interaction, characterized by the sign pattern

$$\alpha = \begin{pmatrix} + & - \\ - & + \end{pmatrix}$$

results in a non-attracting state in which the initial populations remain constant in time. Each population value is then a fixed point, and the phase space motion corresponds to a line of fixed points. On the other hand, the inhibitor–inhibitor interaction

$$\alpha = \begin{pmatrix} - & + \\ + & - \end{pmatrix},$$

Table 1. Activation–inhibition classification of interaction types. The interaction type of a unit in a category is defined by the effect it has on units in the same category (self-interaction), and on units in the other category (cross-interaction).

Type	Self-	Cross-
activator	activator	activator
inhibitor	inhibitor	inhibitor
bigot	activator	inhibitor
loner	inhibitor	activator

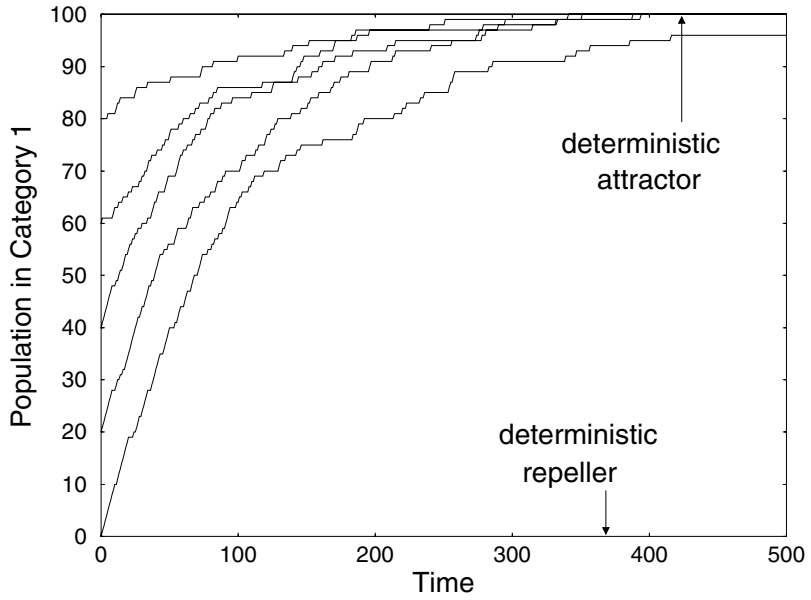

Figure 2. Simulations of a bigot–loner interaction, resulting in positive feedback for the category 1 population. All initial conditions lead to $n_1 = N$ through fluctuating yet monotonically increasing trajectories. $N = 100$, $\alpha_{11} = 1$, $\alpha_{12} = -5$, $\alpha_{21} = 5$, $\alpha_{22} = -1$, resulting in $n_a = 124.75$ and $n_b = -24.75$.

yields continued switching. Thus we find that for the self-interactions, activation arises from $\alpha > 0$ values, and inhibition arises from $\alpha < 0$ (α referring here to matrix coefficients). Conversely, for cross-interactions, inhibition arises from $\alpha > 0$ and activation from $\alpha < 0$.

In the classic activator–inhibitor two-species model [see, e.g., Hofbauer and Sigmund (1991)], the activator species has a positive effect on both itself and the inhibitor species, and the inhibitor has a negative effect on both itself and the activator. This translates into the following sign pattern for our model:

$$\alpha = \begin{pmatrix} + & + \\ - & - \end{pmatrix}.$$

Such dynamics are shown in Fig. 1. It is interesting to note two different asymptotic behaviors that coexist (i.e., multistability) and which can be accessed through

Table 2. Behaviors for the eight symmetric sign patterns of the interaction matrix. The switching behavior determines the dynamics, i.e., the presence of deterministic (det.) or stochastic (stoch.) attractors or repellers. Deterministic attractors are in fact isolated fixed points or lines of fixed points. Lines of fixed points, as in Figs 3 and 5, are here considered attracting when they attract solutions starting outside of their set; however, (constant) orbits starting within the line of fixed points are not stable to perturbations.

Interaction matrix α	Interaction type	Cat1 switch condition	Cat2 switch condition	Dynamical structure
Both categories same interaction types				
$++$ $++$	bigot –bigot	$n_1 < n_a$	$n_1 > n_b$	det. or stoch. repeller
$+-$ $-+$	activator –activator	none	none	det. attractor
$--$ $--$	loner –loner	$n_1 > n_a$	$n_1 < n_b$	det. or stoch. attractor
$-+$ $+-$	inhibitor –inhibitor	all	all	stoch. attractor
Categories different interaction types				
$++$ $+-$	bigot –inhibitor	$n_1 < n_a$	all	stoch. repeller
$-+$ $++$	inhibitor –bigot	all	$n_1 > n_b$	stoch. repeller
$+-$ $--$	activator –loner	none	$n_1 < n_b$	det. attractor
$--$ $-+$	loner –activator	$n_1 > n_a$	none	det. attractor

the choice of initial condition. For the initial population number $n_1(0) > n_a$, the states do not change. We have in this case a line of fixed points extending from n_a to N. Initial conditions less than n_a all lead to an attractor which we describe as 'stochastic': n_1 is a stochastic variable that randomly fluctuates between 0 and n_b; the probability density of the stochastic variable n_1, $P(n_1)$, increases monotonically over the interval $(0, n_b)$. The dynamical origin of the multistability and of the fluctuations in this case will be explained in Section 4.

A traditional 'positive-feedback' interaction pattern requires:

$$\alpha = \begin{pmatrix} + & - \\ + & - \end{pmatrix}$$

with corresponding dynamics shown in Fig. 2. It is clear in this case that the origin is a repellor, and that $n_1 = N$ is a deterministic attractor.

We further introduce two other interaction types or 'species', which we again describe using the activation/inhibition terminology. The 'bigot' is self-activating and cross-inhibiting, i.e., it encourages the proliferation only of those like itself. The 'loner' is self-inhibiting, and cross-activating, i.e., it encourages the proliferation only of those different from itself. All types are summarized in Table 1.

Table 3. Behaviors for the eight asymmetric sign patterns of the interaction matrix. As in Table 2, the interaction matrix determines which dynamical structures will arise.

Interaction matrix α	Interaction types	Cat1 switch condition	Cat2 switch condition	Dynamical structure
$++$ $--$	activator –inhibitor	$n_1 < n_a$	$n_1 < n_b$	$n_b > n_a$ det. attractor stoch. repeller
$--$ $++$	inhibitor –activator	$n_1 > n_a$	$n_1 > n_b$	$n_b < n_a$ det. repeller stoch. attractor
$+-$ $+-$	bigot –loner	none	all	det. attractor det. repeller
$-+$ $-+$	loner –bigot	all	none	
$++$ $-+$	activator –bigot	$n_1 < n_a$	none	det. repeller
$+-$ $++$	bigot –activator	none	$n_1 > n_b$	
$--$ $+-$	inhibitor –loner	$n_1 > n_a$	all	stoch. attractor
$-+$ $--$	loner –inhibitor	all	$n_1 < n_b$	

There are 16 possible sign patterns in all, eight symmetric, and eight asymmetric. For the asymmetric cases, sign patterns can be grouped into pairs within which the roles of n_1 and n_2 are interchanged. Thus there are actually only four distinct interaction schemes for the asymmetric matrices. Tables 2 and 3 show the possible dynamical behaviors for, respectively, the symmetric and asymmetric cases. The behaviors are classified as deterministic or stochastic, and as repelling or attracting.

The correlation between activation and repellor dynamics, and between inhibition and attractor dynamics, is evident from Tables 2 and 3. Intuitively, one can understand that activation, which has a positive effect on the same category and the opposite category, leads to positive feedback and repelling behavior where one population will take over. On the other hand, inhibition, which has a negative effect on both the same and opposite categories, promotes switching back and forth between categories, asymptotically leading to attracting states with or without fluctuations. Below we will comment on the subset of interaction schemes which lead to stable attractors which are of interest for task allocation; in this respect, both symmetric and asymmetric interactions are relevant.

3.3. ***Attractor dynamics.*** The existence of an attractor and its corresponding basins is the predominant dynamical feature of our model. As can be seen from the examples described in our work (Figs 1–5 and Figs 7–8), depending on the interaction matrix α, the attractors can vary widely in type, width, or location, even for the same sign pattern of coefficients. Moreover, these variations produce very

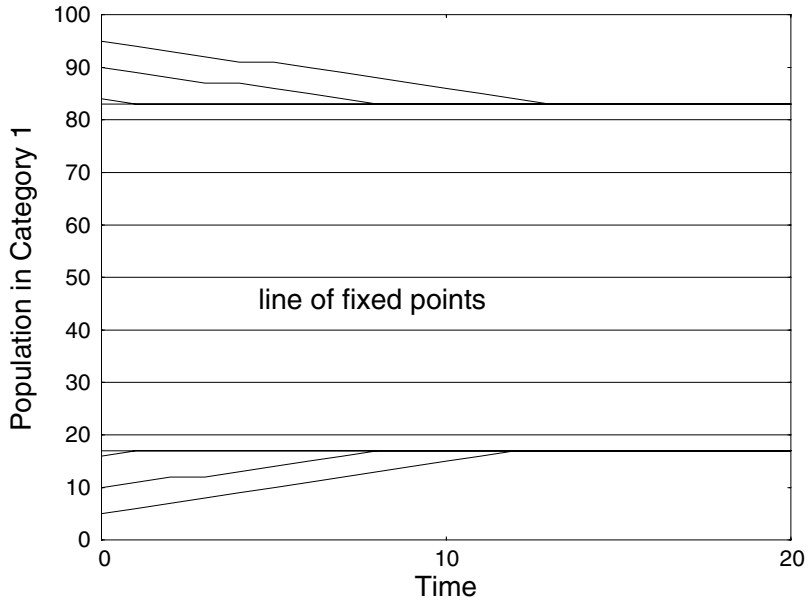

Figure 3. Wide deterministic attractor made up of a line of fixed points from n_a for loner–loner interactions. The fixed points themselves are not stable, but the region $n_b < n_1 < n_a$ attracts all solutions. $\alpha_{ii} = -1$, $\alpha_{ij} = -5$, $n_a = 83.5$, $n_b = 16.5$. The attractor and basins are symmetric about $n_1 = N/2 = 50$. $N = 100$.

different characteristics for the populations, such as stable values, ranges of fluctuations, and rate of decay of perturbations. This is true even though the sign pattern of the matrix may be the same, as we illustrate using the following three examples of *loner–loner* species interactions.

For an interaction matrix with cross-interactions that are large relative to self-interactions, such as

$$\alpha = \begin{pmatrix} -1 & -5 \\ -5 & -1 \end{pmatrix},$$

the dynamics possess a wide line of deterministic fixed points, bounded below by $n_b = 16.5$ and above by $n_a = 83.5$ (Fig. 3). These boundary values attract monotonic trajectories situated, respectively, below n_b and above n_a. Note also that the dynamics are centered about the population value $n_1 = N/2 = 50$; in fact, *symmetric interaction matrices lead to such symmetric dynamical pictures*. Small perturbations to a population (i.e., staying within the attractor) will not be 'corrected' by the dynamics; the population just moves from one fixed point to another. In contrast, large perturbations that bring the population out of the attractor boundaries are kept in check, since they decay monotonically back to the attractor. This case of loner–loner interaction could be appropriate for a situation in which loner units are very inert, the populations remaining mostly fixed and the interactions serving to keep large perturbations of the populations in check.

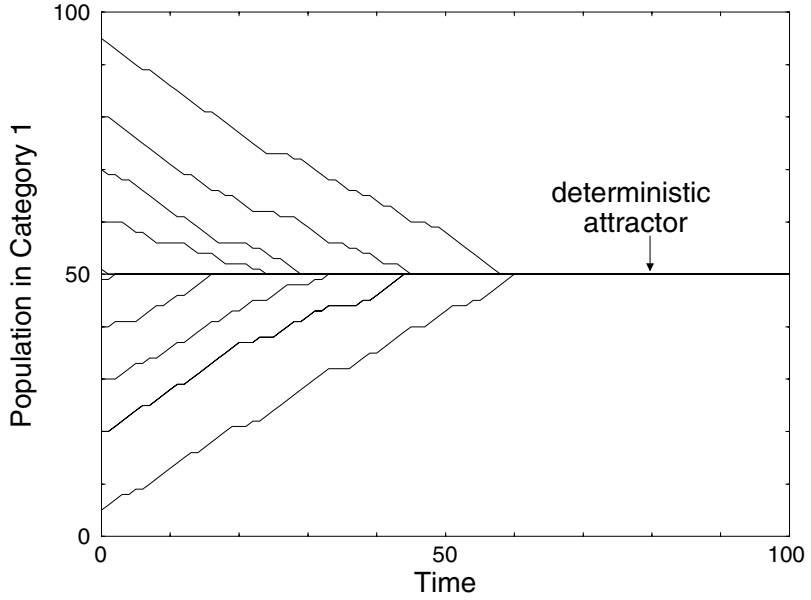

Figure 4. A narrow deterministic attractor center or fixed point arises for a loner–loner interaction with matrix elements $\alpha_{ij} = -1$, $n_a = 50.5$. The critical population values are $n_a = 50.5$ and $n_b = 49.5$. All initial conditions rapidly converge to the equi-population state. $N = 100$.

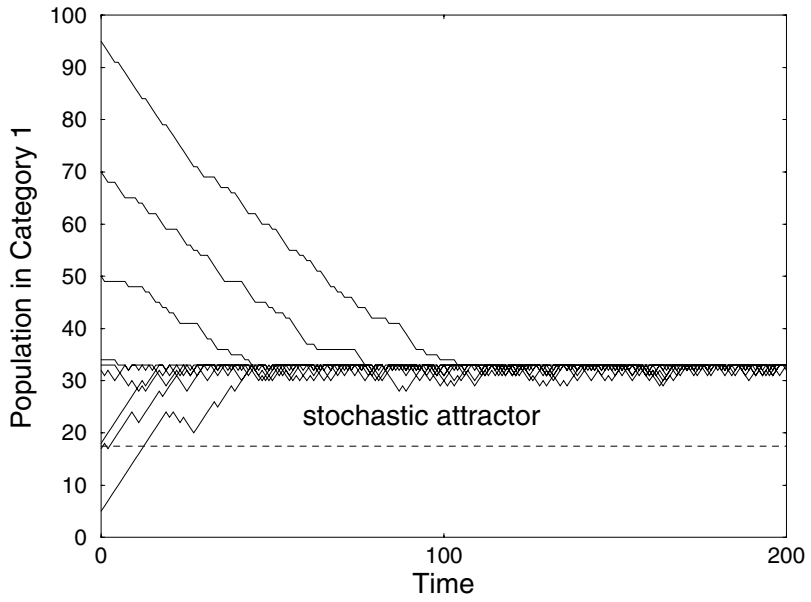

Figure 5. An asymmetric stochastic attractor arises for loner–loner interaction with matrix elements $\alpha_{ii} = -5$, $\alpha_{12} = -1$, $\alpha_{21} = -10$. The critical population values $n_a = 17.5$ and $n_b = 33$, are not centered on $N/2$. All initial conditions converge to solutions that fluctuate persistently near n_b (see also Fig. 9). $N = 100$.

An interaction matrix reflecting equal emphasis on self- and cross-interactions,

$$\alpha = \begin{pmatrix} -1 & -1 \\ -1 & -1 \end{pmatrix},$$

gives a deterministic fixed point at $n_1 = N/2$ due to symmetry (Fig. 4). All perturbations decay monotonically back to $N/2$. This loner–loner interaction allows, solely by means of interactions between units, to control the populations within tight bounds. This case can also be seen as a limiting case of the previous one (Fig. 3).

A loner–loner case with asymmetric ('non-reciprocal') interactions between the units of both categories is

$$\alpha = \begin{pmatrix} -5 & -1 \\ -10 & -5 \end{pmatrix},$$

which leads to the stochastic attractor shown in Fig. 5. The attractor and basin are asymmetrically located with respect to $N/2$, due to the relatively weak activation of units in category 1 by units in category 2. All perturbations decay monotonically back to the stochastic attractor bounded by $n_a = 17.5$ and $n_b = 33$. This case is appropriate to maintain unequal populations within fairly narrow bounds and yet permit the flexibility of constant fluctuation within these bounds.

3.4. ***Rate of decay of perturbations and scaling.*** In this section, we investigate the rate of decay of perturbations for our two-category model, with particular emphasis on the role of the total population N. In the next section, we carry out a similar analysis for random switching dynamics, enabling us to conclude that perturbations in those dynamics decay slower than for our two-category model with state-dependent coupling coefficients. The analysis in Appendix A reveals that the mean of the population n_1 evolves according to

$$\frac{d}{dt}\langle n_1(t)\rangle = \langle t^+[n_1(t)]\rangle - \langle t^-[n_1(t)]\rangle, \tag{5}$$

where t^+ (t^-) is the transition probability per unit time of an increase (decrease) in n_1. For the case of a trapping region with a stochastic attractor, it will be shown in Section 4 that $t^+ = 1 - n_1/N$ and $t^- = n_1/N$. Consequently,

$$\frac{d}{dt}\langle n_1(t)\rangle = 1 - 2n_1/N \tag{6}$$

which has a fixed point at $n_1^* = N/2$. Thus, the location of the attractor scales linearly with N. The relaxation rate onto this fixed point is given by the eigenvalue of the dynamics around n_1^*, i.e., $-2/N$, corresponding to a decay time constant of $N/2$. Thus the decay time simply scales with N. The validity of these scaling behaviors for the equilibrium mean and for the time constant has been verified by

fitting an exponential to responses to perturbations averaged over 1000 realizations (not shown) (each 'realization' being one trajectory with its distinct random updating sequence). However, the probability values themselves do not scale linearly with N; this is not surprising given that numbers of states increase in a binomial fashion with N (see Section 4.2).

3.5. ***Comparison with random switching.*** We may ask to what degree *random dynamics* alone are capable of generating organized behavior. Thus in this section we examine the evolution of category numbers for a random switching rule instead of the deterministic field-based rules used up to now. This will enable us to assess how important the interactions are for producing self-organized population control, as well as to compare speed and tunability of the dynamics.

In the random switching dynamics, a unit is chosen at random at each time step, and it is simply assigned to category 1 with probability p, or to category 2 with probability $1 - p$. The states of the other units do not affect this assignment. Figure 6 shows that, for random dynamics with $P = 0.5$, the mean population converges towards $N/2$. Individual trajectories ('realizations') continually fluctuate around this value. Large perturbations away from this value return to the region, but not monotonically. The set of values that can be taken by n_1 in the asymptotic time limit is the attractor. This attractor corresponds to the whole state space, as we will reason later. Hence, this random switching leads to stochastic attractors that occupy the whole phase space. The probability of finding the different values of n_1 is, however, not uniform, and in fact is peaked around $N/2$.

Let us compare the random dynamics behavior to the dynamics that give stochastic attractors, such as in Fig. 5 (see also Fig. 7). In Fig. 5, n_1 changes by one (upwards or downwards) at each time step; the evolution thus appears jagged. For random switching with $p = 0.5$, the population changes by one only for one-half of the time steps, on average. Evolution is smoother than that in Fig. 5.

Varying the interaction matrix elements causes a shift in the location of the attractor for the field-based dynamics. The location of the most probable population value for random switching can also be shifted by changing the value of p; this is equivalent to introducing a deterministic bias. The random dynamics then lead to an asymmetric probability density over the phase space, with a maximum at $n_1 = pN$ (not shown). Such a stationary probability density is useful to characterize the stochastic process underlying the random dynamics, and to compare model and experimental data; this is true as well for our two-category model, for which we compute densities in Section 4.2. The probability density giving the fraction of the time spent by the system at the value n_1 can be obtained for the random dynamics as follows. We place the states of the N units in a vector labeled from 1 to N. Each state is set to 1 with probability p. The probability $P(n_1)$ that n_1 units are in category 1 is then the binomial

$$P(n_1) = \binom{N}{n_1} p^{n_1}(1-p)^{N-n_1}. \tag{7}$$

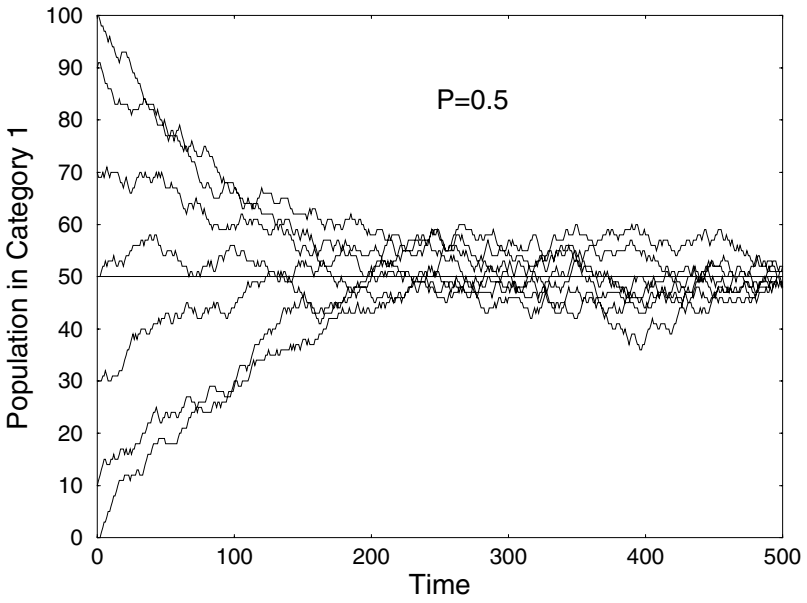

Figure 6. Random dynamics in the two-category network ($N = 100$), with switching probability $P = 0.5$. All initial conditions converge non-monotonically towards the equi-population distribution, about which the solutions exhibit large persistent fluctuations.

This density has mean Np and standard deviation $\sqrt{Np(1-p)}$. Also, for N large and Np large, the binomial can be approximated by a Gaussian density with the same mean and standard deviation. Hence, the density is approximately Gaussian for the random dynamics under these conditions, which is the case for Fig. 6.

However, the random dynamics can*not* be 'tuned' to make the fluctuation region narrower; the fluctuations are always present, and can bring the trajectory anywhere in phase space. Further, since evolution is never monotonic, perturbations take longer to die out. This can be further verified by comparing the speed of recovery from perturbation for the two dynamics. As in the previous subsection, this can be done using the formalism of Appendix A [equation (5) or equation (A10)]. For random switching dynamics, the probability $t^-(n_1)$ that n_1 decreases by one in a time step is given by the probability of choosing a category 1 unit (n_1/N) times the probability of changing it to a category 2 unit, which is $(1-p)$. Conversely, the probability $t^+(n_1)$ that n_1 increases by one in a time step is given by $p(1-n_1)/N$. The mean of the corresponding birth–death process thus evolves as $dn_1/dt = (p-n_1)/N$, with a fixed point at $n_1^* = p$, as expected, and decay ('recovery') time constant equal to N. These scaling behaviors for the fixed point and the time constant have also been verified numerically using trajectories obtained by ensemble averages over many (1000) realizations of the model (not shown). Attractor location thus depends solely on p, and the recovery time is twice as long as for the field-based rules.

In summary, random dynamics can reproduce some of the important features of the two-category model with certain interaction matrices, namely the return to a neighborhood of some (chosen) population value, with intrinsic fluctuation about that value. What random dynamics cannot do is reduce the range of n_1 values over which the solution fluctuates to an arbitrary level, nor demonstrate fast monotonic return of the mean population n_1 back to its steady-state value. The particulars of the biological system to be modeled will dictate whether random dynamics are sufficient to explain the experimental observations, or whether interactions are required.

3.6. ***Summary of couplings that produce attractors.*** In this subsection, we summarize the dynamics that lead to either deterministic or stochastic attractors for the intrinsic dynamics (i.e., without external forcing). The interactions that give rise to these attractors are then potential 'coupling candidates' for task allocation. We write 'potential', because a full analysis of network dynamics in the presence of a variety of external stimuli is required before one can narrow the field of possible couplings that underlie task allocation in a given context, e.g., in a given ant species. However, we note that our preliminary analysis of the dynamics of our model with added coupling between ants and an external environmental stimulus (such as a food source) reveals that the same behaviors as those summarized here occur, as long as the stimulus does not become too strong, and n_a and n_b are not too close; in fact, since n_a and n_b vary with the stimulus level, their ordering may change with time which generally leads to switches between qualitatively different dynamics.

We can make a first summary based on the number of positive and negative coupling coefficients. As mentioned in Section 3.2, activation tends to be associated with repellors, and also lines of fixed points, while inhibition tends to lead to attractors. In particular, one can see from Tables 2 and 3 that more than two negative signs in the coupling matrix leads to attractors; more than two positive signs leads to repellors. And equal numbers of both signs are borderline cases that can lead to either attracting or repelling dynamics. Inhibitory cross-interactions lead to a deterministic attractor (which may in a few cases coexist with a repellor); and self-inhibition tends to lead to stochastic attractors (except for certain cases with two negative and two positive signs).

Of the 16 possible activation/inhibition sign patterns, we find that as many as four produce stable but fluctuating ('stochastic') population dynamics (Tables 2 and 3). These sign patterns, two symmetric and two asymmetric, correspond to three different types of interaction pairs, viz., loner–loner (symmetric), inhibitor–inhibitor (symmetric), and inhibitor–loner (or loner–inhibitor) (asymmetric). Furthermore, the asymmetric borderline activator–inhibitor case (or inhibitor–activator) may yield a stochastic attractor that coexists with a deterministic repellor when $n_b < n_a$. *Our model thus predicts coupling conditions where intrinsic fluctuations occur, which could add to other sources of noise (such as sampling errors), and which*

Table 4. Attractors for loner–loner interaction.

Figure	α matrix	Attractor type
3	$\begin{pmatrix} -1 & -5 \\ -5 & -1 \end{pmatrix}$	symmetric, deterministic, wide
4	$\begin{pmatrix} -1 & -1 \\ -1 & -1 \end{pmatrix}$	symmetric, deterministic, narrow
5	$\begin{pmatrix} -5 & -1 \\ -10 & -5 \end{pmatrix}$	asymmetric, stochastic, narrow
8	$\begin{pmatrix} -2 & -1 \\ -1 & -2 \end{pmatrix}$	symmetric, stochastic, wide

may account for some of the experimentally observed fluctuations. This is true for task allocation, and more generally for networks, neural and other, which evolve according to these coupling rules.

Other attracting dynamics that are interesting for task allocation are those that produce deterministic attractors. They are, for the symmetric cases: activator–activator, loner–loner, activator–loner, loner–activator. For the asymmetric case, we have bigot–loner, and as before, the activator–inhibitor (or inhibitor–activator) case when $n_b > n_a$.

We illustrate our findings by highlighting two couplings that lead to typical kinds of attractors. The first coupling is loner–loner, which leads to a variety of deterministic and stochastic attractors depending on the magnitude of the coupling coefficients (see Table 4). The sign pattern is:

$$\alpha = \begin{pmatrix} - & - \\ - & - \end{pmatrix}.$$

For the chosen α values of Fig. 7, a symmetric stochastic attractor is generated (cf. asymmetric stochastic attractor of Fig. 5). The category populations are controlled deterministically at high and low values by a *monotonic return* to the attractor region. The population then fluctuates around $N/2$. Other loner–loner attractors (for other values of α) can contain constant ('stalled') states as well (e.g., Figs 3 and 4).

The matrix for the inhibitor–inhibitor pair,

$$\alpha = \begin{pmatrix} - & + \\ + & - \end{pmatrix},$$

also yields a stochastic attractor that spans the whole phase space (Fig. 8). This is similar to the random switching dynamics of Section 3.5. One difference, however, is the presence here of switchings at each time step; in contrast, the random switching rule did not produce changes in n_1 at each time step. The populations are controlled here *not* by attractor boundaries or basins, but by the (random) selection of units for updating. The category to which the chosen unit belongs here matters, which is not the case for random switching. This leads, as we have seen

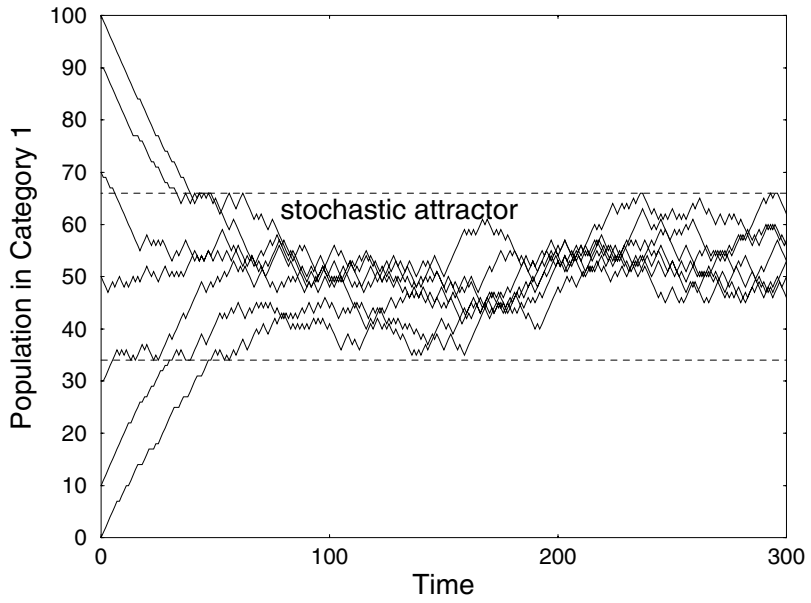

Figure 7. A symmetric stochastic attractor arises for loner–loner interactions with matrix elements $\alpha_{ii} = -2$ and $\alpha_{ij} = -1$. All initial conditions converge monotonically to the attractor, itself characterized by large fluctuations. Here $n_a = 34$ and $n_b = 66$ with $N = 100$.

in Section 3.5, to faster decay of perturbations in comparison with the random switching case.

In summary, the interaction schemes summarized in this section produce attractors that are either deterministic or stochastic, symmetric or asymmetric, and with or without attractor edges. In particular, the fluctuating behavior around the mean is similar in all the stochastic cases. It is in the behavior far from the mean (and for certain cases, outside the attractor) that the difference between population control strategies is most apparent. *Also, we find that all the species (inhibitors and loners) which qualify for self-organized task allocation are self-inhibiting* (only one of the two is self-inhibiting in the borderline case of activator–inhibitor or its reverse). Such a prediction could also serve to test the model experimentally.

4. ITERATED FUNCTION SYSTEM AND BIRTH–DEATH FORMULATIONS

Comparisons between model predictions and experimental data are difficult to make if: (1) the dynamics have a significant component of randomness, and/or (2) the experimental data itself exhibits fluctuations. Model validation in the steady state can nevertheless be done by comparing, e.g., first and second moments of fluctuating time series, or better still, the whole probability density of various state variables. The computation of this density and the origin of the basin structure

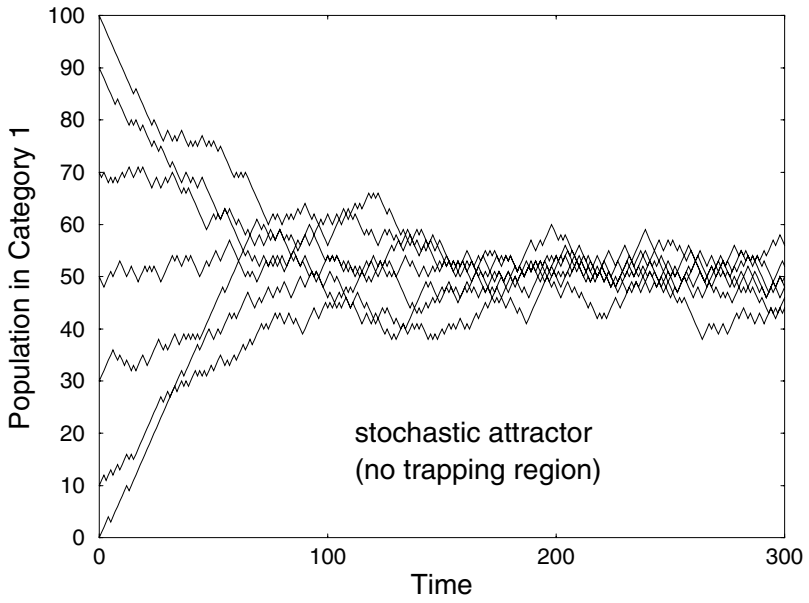

Figure 8. A stochastic attractor arises for inhibitor–inhibitor interactions with matrix elements $\alpha_{ii} = -2$ and $\alpha_{ij} = 1$. All initial conditions converge non-monotonically but rapidly (cf. random dynamics in Fig. 6) towards the equi-population value but fluctuations persist. Here $n_a = -98$ and $n_b = 198$ with $N = 100$.

covered in Section 3 are the subject of this section. The results of our analysis further yield insight into the dynamical nature of the stochastic attractors. One of our main results is that the constrained motion on 'stochastic' attractors is in fact a random walk through a specific (and calculable) part of the population number phase space, with probabilities of stepping to the right (increasing n_1), to the left or of standing still being a function of the current population. *By extension, this result implies that such state-dependent random walks are equally at work in the Gordon et al. model (1992), but their analysis is complicated there by the presence of three fields (rather than one here)*; further elaboration of our work to more than two categories is currently under investigation.

We first show that the dynamics of our model can be formulated in terms of an iterated function system (IFS). The IFS representation leads to a deeper understanding of the dynamical behaviors exhibited by our model and, in particular, explains the basin structure we have observed numerically. In addition, the IFS representation suggests a subsequent one, based on a birth–death master equation. This latter formulation enables us to predict, among other things, the probability distribution of the category numbers.

4.1. ***The two-category model as an iterated function system.*** We begin by establishing that the two-category model behaves as an IFS. In our model, units are updated asynchronously, with one unit being randomly selected at a given time

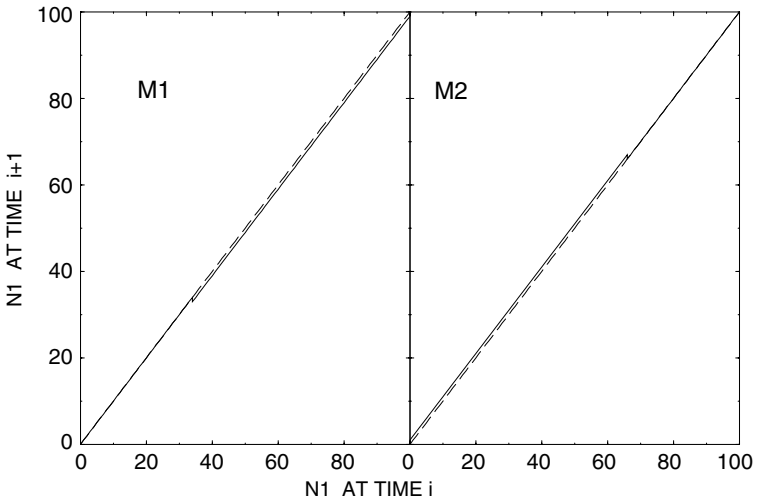

Figure 9. Representation of the dynamics of the network model in terms of an iterated function system composed of two deterministic maps. At each time step, either the number of ants in category 1 is updated using the map M1 on the left, or the number of ants in category 2 is updated using the map M2 on the right. Which map is used at a given time step is determined randomly, with a probability that is a function of the number of ants n_1 in category 1. Note that, in each case, the maps (solid curve) are either the identity function (the diagonal, represented by a dashed curve), or a value that deviates from the identity by one. The maps were generated using the parameters for Fig. 7, for which $n_a = 34$ (the break point in the M1 map) and $n_b = 66$ (the break point in the M2 map).

step. This unit can be either in category 1 or 2. Switching between categories is governed by the deterministic field-updating rules of Section 2.1. If the unit chosen at a given time step is in category 1, the number of category 1 units, n_1, can either decrease or stay the same. Alternatively, if it is in category 2, the number n_1 can either increase or stay the same. The parameters n_a and n_b, which are functions of the interaction matrix elements, thus set boundaries between 'change' and 'no change'.

We can summarize these rules using two maps, one for each category. This is shown in Fig. 9 using the parameters for Fig. 7; *however, our analysis is valid for any matrix elements.* If the chosen unit is in category 1 (2), the next value of the population n_1 will change as a function of the current value according to the map on the left (right) in Fig. 9. The break points in the curves occur, respectively, at $n_1 = n_a = 34$ for the M1 map (associated with category 1), and at $n_1 = n_b = 66$ for the M2 map (category 2). Note that the abscissa (i.e., the domain $0 \leq n_1 \leq N$) is the same for both maps. An interval of the domain over which the curves for each map have a given shape will correspond to a certain dynamical behavior.

For example, in Fig. 7, for $0 \leq n_1 \leq n_a$, the M1 curve is the identity, while the M2 curve is the identity plus one. This corresponds to the following behavior: if a category 1 unit is chosen, do nothing; if a category 2 unit is chosen, increment n_1 by one (i.e., switch the unit to category 1). Hence, when n_1 is in this interval,

the value of n_1 remains either constant or it increases, in agreement with Fig. 7. Likewise, for $n_b \leq n_1 \leq N$, n_1 stays constant or decreases. Both these intervals constitute the basins of the attracting region $n_a \leq N \leq n_b$, which as we can see simply from these maps, is the trapping region found in Fig. 7.

In this trapping region, n_1 either increases by one (if category 2 is chosen) or decreases by one (if category 1 is chosen). This leads to a random walk for n_1; thus, in this case the dynamics are in fact stochastic. However, *and this is the crux of the matter*, the probability of stepping to the right or left, i.e., of increasing or decreasing n_1 by one, depends on the current value of n_1. In other words, the dynamics in this trapping region are similar to a random walk with state-dependent biases. In particular, the state-dependent biases for our model in Fig. 7 produce a greater driving force towards the center $N/2$ than for the random dynamics in Fig. 6.

The reason for these state-dependent biases lies in the fact that the probability of using M1 is n_1/N, i.e., the probability of choosing a unit in category 1. Likewise, the probability of using M2 is $\left(1 - \frac{n_1}{N}\right)$. Hence, the following dynamical picture emerges: the dynamics evolve according to a random sequence of choices between two deterministic maps, with the probability of choosing between these maps at the beginning of each time step being a function of n_1 at the beginning of each time step. When n_1 is large (small), M1 is chosen more (less) often. This type of dynamical system is an iterated function system with state-dependent probabilities, and has been studied in, e.g., Barnsley *et al.* (1985).

All the behaviors of our two-category model can be analyzed using this iterated function representation. For example, the regions referred to as 'lines of fixed points' (see, e.g., Figs 1 and 3) correspond to phase space intervals where M1 and M2 are the identity function on overlapping subdomains; thus, regardless of which category the chosen unit belongs to, the value of n_1 does not change over a time step, i.e., it is a fixed point. Also, the explosive 'positive feedback' behavior seen in Fig. 2 occurs because $N < n_a = 124.75$, $n_b = -24.75$; this leads to M1 being the identity over $0 \leq n_1 \leq N$, and M2 being the identity plus one over the same domain. Thus, n_1 increases or stays constant; and as n_1 approaches N, the M1 'identity' map is chosen more often, until the globally attracting fixed point $n_1 = N$ is reached.

4.2. ***The two-category model as a birth–death process.*** The fact that the population n_1 changes by a random yet finite amount at each time step suggests that the dynamics are similar to a stochastic process known as a one-dimensional birth–death process [see, e.g., Gardiner (1985)]. Further, the fact that the probability of births (increasing n_1 by one) or deaths (decreasing n_1 by one) varies as a function of the state variable suggests that the transition rates in the birth–death process are state-dependent. Here we show that this similarity can be exploited to derive the probability density for the stochastic variable n_1 in the steady state. We confine our discussion to the trapping regions of Figs 5 and 7; an identical analysis can be applied to all the behaviors found in our study.

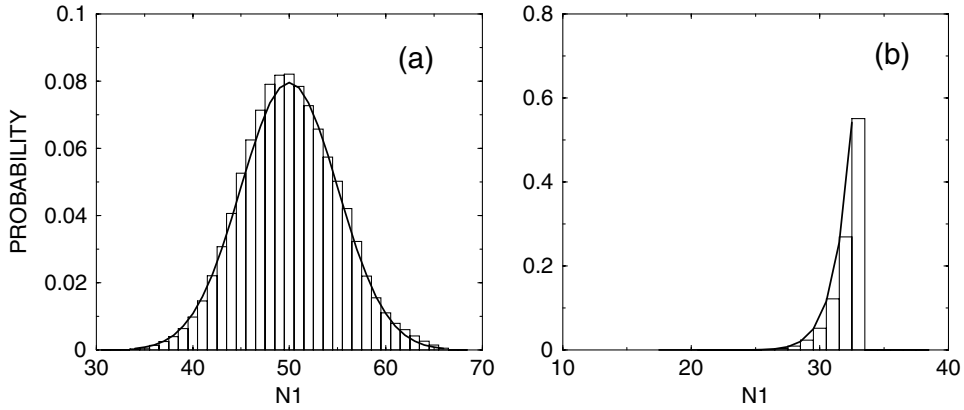

Figure 10. Normalized probability density of the number of ants in category 1, for the parameters corresponding to (a) Fig. 7 and (b) Fig. 5. The histograms were obtained from iteration of the model for 30 000 time steps, discarding the first 1000 time steps as transients. Superimposed on the histograms (solid curves) are, for each case, the theoretical normalized probability density predicted from our analysis of the two-category model in terms of a birth–death jump process. In both cases, the agreement is seen to be excellent within statistical fluctuations.

Later we use the stochastic variable x in place of n_1. The birth–death system is characterized by the conditional probability $P(x, t|x_0, 0)$, where x_0 is the initial population at time t_0 (t_0 is chosen here to be zero). This probability evolves according to a 'master equation'; this equation is described and solved for its asymptotic density $P_s(x)$ for the special cases of Figs 5 and 7 in Appendix A. This steady-state probability density $P_s(x)$ is plotted in Fig. 10 alongside the density obtained from numerical simulations of our two-category model for the parameters of Figs 5 and 7. The agreement is seen to be excellent, as expected, since this is an exactly solvable model. It is also seen that the density in Fig. 10(a) has a bell-shape, and a truncated bell-shape in Fig. 10(b).

It is interesting to note the simplicity of the resulting density: the probability that the population n_1 has a certain value x at a given time (in the allowable range bounded by n_a and n_b) is proportional to the number of ways of choosing x units out of N units, i.e., the standard binomial coefficient. Note also that the density differs from the standard 'binomial distribution', found, e.g., here in our study for the random switching dynamics in Section 3.5, since the latter further involves the factor $p^{n_1}(1-p)^{N-n_1}$.

That fact that the density is proportional to the number of possible ways of choosing x elements out of N elements also establishes a link between the dynamics of such networks and the 'entropy' encountered in classical statistical mechanics and information theory [see, e.g., Pathria (1984)]. There, the entropy of a given macrostate, i.e., a state characterized by macrovariables such as the value n_1 in our context, is proportional to the number of associated microstates compatible with this microstate. In our case, a microstate consists of the specification of the state

of each of the N units, the units being distinguishable. Hence, our analysis reveals that the macrostate of highest probability is that to which corresponds the largest number of microstates, i.e., the largest entropy. Although our mean-field model is concerned only with macrostates at this point, these entropy considerations are likely to be useful for extensions of our work to account for the spatial distribution of interacting units.

Assuming that the time step equals unity, the iterated function analysis previously discussed further suggests the following evolution of the mean of x for the general case (neglecting fluctuations):

$$\frac{dx}{dt} = \frac{x}{N}(H[F_1(x)] - 1) + \left(1 - \frac{x}{N}\right)H[F_2(x)], \tag{8}$$

where F_1 and F_2 are the fields defined in Section 2.2, and H is the Heaviside function, $H[F < 0] = 0$, $H[F > 0] = 1$. For the cases of Figs 5 and 7, our analysis in terms of maps, or the analysis of the equation above, reveals a trapping region with a stochastic attractor. In that region, the mean number of units in category 1 is obtained by solving the equality between right and left transition probabilities per unit time (see Appendix A): $t^+(x^*) = t^-(x^*)$, i.e., $x^* = N/2$. Intuitively, the behavior of the mean is like the highly damped motion of a particle in a parabolic potential; however, this motion is constrained by the reflecting boundaries of the trapping region.

Interestingly, the birth–death formalism is also used to study chemical reactions in systems of atoms and molecules. Switching according to mean field rules and state-dependent coefficients thus embodies a kind of 'task allocation chemistry', where molecules change their properties and composition via reactions, and the course of these reactions in turn depends on the properties of the different kinds of molecules. The formalism also enables the computation of correlation functions and other temporal properties of the solutions. These properties, as well as their generalization to more than two categories, will be left for future work.

5. Two-category Dynamics with an External Stimulus

Up to now, we have only considered the behavior of the two category model in its autonomous regime, focusing solely on the effect of the interaction matrix on population numbers. A more general theory for the behavior of such neural networks should include the combined effect of these autonomous dynamics along with the response to external stimuli (Bonabeau *et al.*, 1998a; Gordon, 1999a). In the context of insect colonies such as harvester ants, these stimuli can relate, e.g., to specific colony needs and/or to the influence of external factors such as the availability of food sources. Another obvious external stimulus is the position of the sun, since it is known that colony behavior varies according to a circadian clock (Gordon, 1999a). In the context of neurons, the external stimulus is simply

any activity that drives the network from outside its boundary; it may arise from another group of neurons, or from physical stimuli such as sound. The main focus of our paper has been on the dynamics arising from interactions between units, because of the lack of knowledge about such dynamics in the literature. In this section however, we describe some interesting findings on the stimulus driven two-category dynamics; a full account of such dynamics will be given elsewhere.

It is straightforward to extend our model to account for the effect of external time-dependent stimuli. This can be done either by introducing a bias term in an appropriate field, or alternatively, by making the threshold for a given field vary with the stimulus associated with that field [see, e.g., Bonabeau *et al.* (1998a)]. The level of an external stimulus could be independent of the category numbers (such as for the circadian activity), in which case the category numbers would be enslaved to the particular time variations of the stimulus. In our model, this simply leads to temporal variations in the parameters n_a and n_b that are enslaved to the stimulus. The model dynamics then simply boil down to what we already know from the previous sections, with, however, the added possibility that attractors as well as their boundaries move around in time. Note, however, that n_a and n_b can cross, which may lead to qualitative dynamical changes (see later).

The dynamically more interesting case is the one in which the stimulus is a time-dependent function of the number of ants performing a task relevant to that stimulus. The model would then induce couplings between categories via stimuli (Bonabeau *et al.*, 1998a), as well as via the intrinsic direct interactions between categories which have been the focus of our work up to now. We consider one external stimulus $s(t)$, which increases at a constant rate I and decreases at a rate $\gamma n_1/N$, i.e., a rate that depends on the number of ants performing the task (arbitrarily) associated with category 1:

$$s_{i+1} = s_i + I - \gamma * n_1/N \tag{9}$$

where the label i denotes discrete time. Further, we require (arbitrarily) that a strong stimulus motivate more ants to switch to category 1. This is achieved by reducing the threshold for ants in category 2 to switch to category 1, and by increasing the threshold for category 1 ants to switch to category 2 ants. The critical populations n_a and n_b in Section 2.2 now become time-dependent:

$$n_{a_i} = [-s_i + \alpha_{11} + \alpha_{12} * N]/(\alpha_{11} + \alpha_{22}) \tag{10}$$

$$n_{b_i} = [-s_i + (N-1) * \alpha_{22}]/(\alpha_{21} + \alpha_{22}) \tag{11}$$

It is clear from equation (9) that, if the mean of the stimulus reaches an equilibrium value, the mean of n_1 will reach a value around IN/γ. This is shown in Fig. 11 for the same intrinsic parameters as in Fig. 1. For this specific case, switches from category 1 to category 2 occur if $n_1 < n_a$, and from 2 to 1 if $n_1 < n_b$. Note that the initial values for the boundary parameters, n_{a_0} and n_{b_0} also depend now on the initial value of the stimulus s_o. Further, n_a and n_b are bounded on one side by their

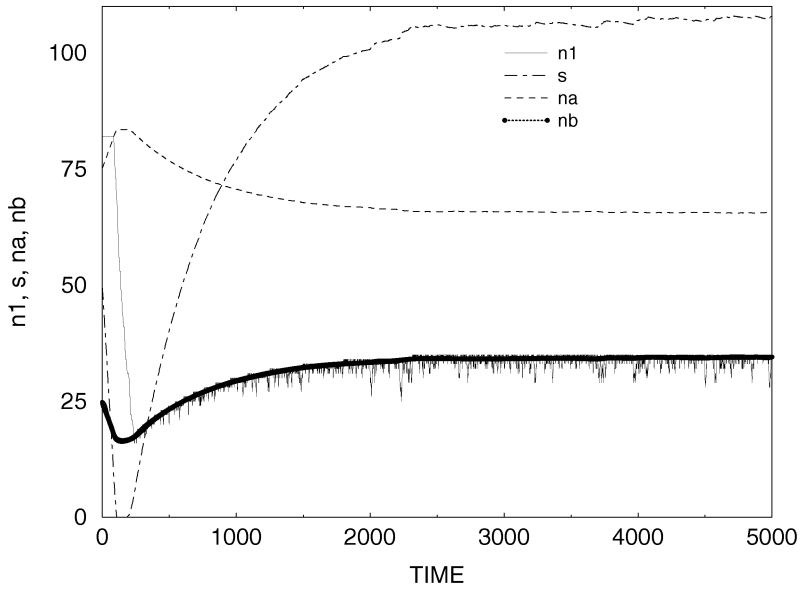

Figure 11. Population of category 1 units (n_1) vs time for the activator–inhibitor coupling matrix of Fig. 1, in the presence of an external stimulus (s) that evolves according to equation (9) (see Section 5). Also plotted are the critical populations n_a and n_b. Other parameters are the initial population of category 1, $n_0 = 82$, the initial stimulus strength $s_0 = 50$, the rate of increase of the stimulus $I = 0.34$, and the decay factor $\gamma = 1.0$. Note that asymptotically, n_b lies at the upper bound of the n_1 time series.

values for zero stimulus; so if the parameters for the stimulus evolution are such that the stimulus reaches zero in the steady state, the dynamics of n_1 will tend to those that prevail in the absence of stimulus.

Numerical simulations for Fig. 11 reveal that there are now a number of possible kinds of dynamics, depending on the choice of parameters. The picture is in fact more complex than without stimulus. But for certain parameter sets, the dynamics are essentially the same. Specifically, initial conditions beyond n_a will remain constant (line of fixed points), but the lower boundary n_a of this line may vary in time. Likewise, the boundary n_b will vary. Note that in Fig. 1 $n_a = 83.5$ and $n_b = 16.5$. One can also understand, using the analysis in terms of the iterative function systems (Section 4.1), that n_1 tends to the lower boundary n_b. Consequently, we have that $n_1^* \approx n_b^* \approx IN/\gamma = 34$. This is approximately the upper bound of n_1 in Fig. 11. Substitution into equation (11) yields an equilibrium stimulus strength of $s = (N-1)\alpha_{22} - (\alpha_{21} + \alpha_{22})IN/\gamma \approx 104$ and $n_a \approx 66$, as observed.

Thus, in the presence of an external stimulus that drives switches of ants to category 1, the resulting dynamics in Fig. 11 are 'qualitatively' similar to those without external stimulus: the attractor is asymmetric with fluctuations occurring below a value around (the new value of) $n_b^* = 34$. We have found that this is generally true for the different dynamics encountered in our study, as long as the stimulus growth

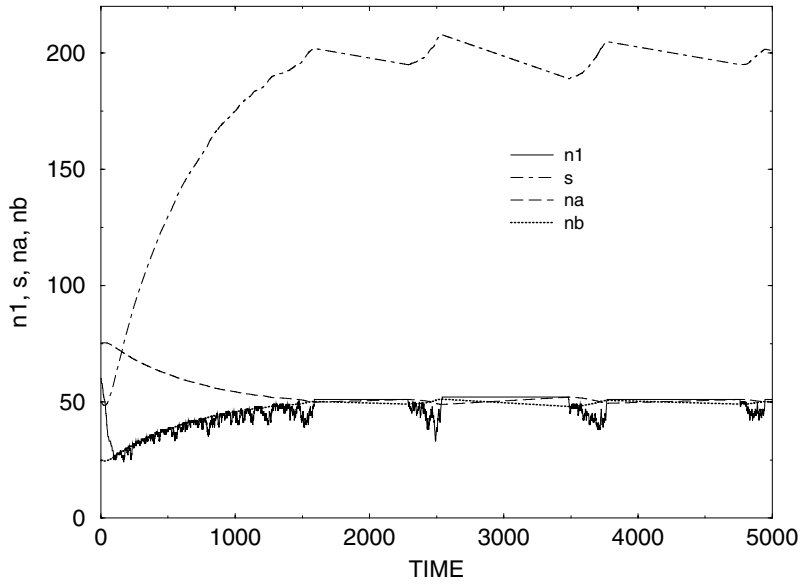

Figure 12. Same as for Fig. 11, except that $n_0 = 60$ and the stimulus rate of increase is higher at $I = 0.5$. The critical populations n_a and n_b evolve from their initial values of 75.2 and 24.8, respectively, and cross each other repeatedly over time, leading to qualitative shifts in the dynamics.

is not too large compared to its decay, and as long as n_a and n_b are not too close to one another. If, for example, an initial stimulus strength makes these boundaries close, the resulting evolution may make them cross more times, leading to quite different dynamical behaviors in comparison to the case without external stimulus. The same is true if n_a and n_b are already close without stimulus; then, even a small initial stimulus strength can reverse the ordering of n_a and n_b, leading again to qualitatively different dynamics. A case where the two values cross repeatedly is shown in Fig. 12.

In summary, our model can be used to explore the dynamics with both ant–ant interactions and interactions between ants via an external stimulus whose decay rate depends on the number of ants in a certain category. This can be extended to higher numbers of categories as well. The full classification of the interaction matrices for situations with such an external stimulus will be an arduous task; but at least the dynamics can be decomposed into those found for the model with ant–ant interactions alone. And these behaviors will prevail when stimulus strength is not too large and the critical population numbers are suitably distant.

6. DISCUSSION AND OUTLOOK

6.1. ***Summary of two-category network dynamics.*** In this paper we have uncovered and analyzed the rich dynamical behavior of a two-category network model of task allocation without central control. We were able to determine the full reper-

toire of dynamical behaviors as a function of the interaction matrix. We found that the sign patterns of the interaction matrices (eight symmetric, eight asymmetric) could be usefully classified into a limited number (10) of category interaction types using the notion of 'activator' and 'inhibitor' for the self- and cross-interactions. We then showed how particular category interaction types determined the characteristics of the resultant behavior in the long-time limit, i.e., of the 'attractor' behavior. Some of these attractors (summarized later) exhibited continual fluctuations in a bounded domain determined by the critical population numbers n_a and n_b. These intrinsic fluctuations are one prediction of our model with respect to the sources of variability in measurements of population numbers for different tasks.

The attractors were described by defining and analyzing features such as their stability, boundaries, deterministic vs stochastic nature, location, width, the monotonicity of their transient solutions, and the rate of decay of perturbations. All these features can be obtained from time series data of category population numbers, and thus direct comparisons between data and model are possible. We also studied a number of general features of our network model. We found that symmetric interactions, where the coupling coefficient of category 1 with category 2 is the same as for category 2 with category 1, lead to symmetric dynamical pictures in phase space. Also, for two categories, a maximum of two coexisting long time behaviors (each accessible via a specific set of initial populations) could occur. Comparison of our model to one based on random switching further revealed that the latter can capture some of the stochastic behavior of category switching dynamics, but few of the more desirable 'self-regulation' aspects of our model, such as narrow attractor widths or fast monotonic returns. Our analysis in fact revealed that our model exhibits rates of decay of perturbations that are twice as fast as for random switching dynamics (Sections 3.4–5).

We further determined the conditions on the interaction matrix which lead to dynamically stable behavior of the category populations, with a chosen mean equilibrium value dependent on coupling parameters to other units and to the environment, and recovery from perturbations. We isolated a number of category interaction types, viz. loner–loner (Figs 5 and 7), inhibitor–loner (Fig. 9), and inhibitor–inhibitor (Fig. 8), all of which yield stochastic attractors, as candidates for task allocation models. We have also identified those interactions that lead to deterministic stable attractors. Also, the activator-inhibitor scheme (Fig. 1) can, for certain parameters, produce a stochastic attractor.

Finally, we have given preliminary analyses of the kinds of behaviors that can arise when the units respond to an environmental stimulus such as a food source that can be altered by the ants in a given category (such as the active ones). We have modeled this response via its effect on the switching thresholds. The same qualitative behaviors as without such a stimulus (i.e., those described in Section 3) are found when the stimulus does not dominate the dynamics (Section 5); otherwise, there can be alternations between qualitatively different dynamical behaviors over time.

6.2. ***Mathematical insights into non-hierarchical task allocation.*** Despite the simplicity of its network architecture, our model is capable of producing a startling variety of behaviors. Isolated fixed points, neutrally stable lines of fixed points with a basin of attraction, stochastic attractors characterized by fluctuations in a bounded area of population number space, and transients that decay either monotonically or not onto the aforementioned attractors, are the key behaviors of our model.

We also proposed an analysis of the two-category model using an iterated function system, which allowed us to understand the origin of attractor basins and the nature and robustness of the different kinds of attractors. This in turn led to a birth–death process analysis, which enabled us to exactly compute the probability density of the fluctuations seen, e.g., in the trapping regions of Figs 5 and 7. The dynamical picture of non-hierarchical task allocation that emerges is then one in which the interaction matrix coefficients establish phase space boundaries n_a and n_b; the particular signs of the coefficients, along with the initial conditions, then determine whether the long-time dynamics are constant, or a biased random walk. As the biases of this 'walk' (increasing, decreasing, or constant) are themselves dependent on the current population number, these walks lead to various kinds of stochastic attractors characterized by their location, width, symmetry, number of underlying 'microstates', and basin(s) of attraction.

This birth–death formalism could also be used to compute temporal properties of the solutions, such as the autocorrelation of the fluctuations within one category, or the cross-correlation between the fluctuations of two categories (in our two-category model, this latter cross-correlation is obviously trivial). We anticipate that our analysis will further enable us to study category switching and perturbation propagation between categories in models with two or more categories. In fact, our theoretical and numerical analyses together suggest that the complexities exhibited by the eight-category model (Gordon *et al.*, 1992; Torres and Trainor, 1993), and more generally, by network dynamics with state-dependent coupling coefficients, are of the same nature as those found in our two-category model. Although the analysis in not likely to be straightforward, it is expected that the phase space of a higher-dimensional model will also be parceled into (perhaps more) subregions by boundaries (hyperplanes), with stochastic motion arising in certain regions, analogous to higher-dimensional random walks with state-dependent biases.

6.3. ***Possible extensions of our model.*** It is possible to extend our model to account for more aspects of the biological reality. In the context of task allocation in harvester ants, there exist empirical data as well as other modeling studies that can motivate these extensions, and especially provide estimates for model parameters. Here we discuss a few possible extensions. We first consider the effect of the sampling fraction, which was set equal to one in our analysis. We then discuss the incorporation of 'contact rate' with other ants. We then speculate on other aspects of the model that would be interesting to pursue in future studies.

6.3.1. *Sampling fraction.* In Section 2.2, we have chosen to compute the field as in Gordon *et al.* (1992), i.e., by using an average over the whole ant population. However, an ant is not expected to use input from every other ant for its updating procedure. Instead, it may sample a certain fraction $0 < c < 1$ of the whole population. Assuming again that the categories are well-mixed, such as near the entrance of the nest, the expression for the field then becomes:

$$F_i = \sum_{k=1}^{2} c\, n_k \alpha_{ik} S_k - \alpha_{ii} S_i .$$

The general dynamical properties of the model remain basically unchanged except for the fact that the critical population numbers are now:

$$n_a = \frac{\alpha_{11} + cN\alpha_{12}}{c(\alpha_{11} + \alpha_{12})}, \qquad n_b = \frac{(cN - 1)\alpha_{22}}{c(\alpha_{22} + \alpha_{21})}.$$

Thus, the sampling parameter c will change attractor boundaries in a way that depends on the sign of the interaction matrix coefficients and on N. This can have important consequences for the characteristics of the attractors such as location, width and basin structure. For example, if c is small, the magnitudes and even signs of n_a and n_b may be altered, leading to perhaps totally different dynamics with respect to the $c = 1$ case. One could even imagine that c is a stochastic variable, making n_a and n_b intrinsically stochastic variables as well. The result is then that these critical populations will fluctuate in time, causing effects similar to those seen when they fluctuate because of external stimuli (Section 5).

Nevertheless, the same kind of attractors as for $c = 1$ will be produced by our model with c less than but close to 1. For example, for Fig. 7, a sampling fraction of 0.1 rather than 1 leads to the same kind of stochastic attractor (not shown); the only difference is that the boundaries are moved to $(n_a, n_b) = (40, 60)$ from $(34, 66)$, i.e., the attractor is narrower. We note as well that as N increases [cf. a colony of harvester ants can reach a population upwards of 10 000 after many generations—see Gordon (1999a)], the excluded interaction of an ant with itself as well as the sampling fraction c become insignificant determinants of the behavior of the model. In fact, for large N, $n_a \approx N\alpha_{12}/(\alpha_{11} + \alpha_{12})$ and $n_b \approx N\alpha_{22}/(\alpha_{21} + \alpha_{22})$. These changes in dependency as N increases in our model agree with our intuition that the estimate of the field for large N should not depend sensitively on which ants are met; a 'mean field' can be accurately estimated from a fraction of the ants.

6.3.2. *Asynchronous updating and contact rate.* In our model, updating is asynchronous. One time step corresponds to the mean interval between one ant in the population assessing the task cue (e.g., a pheromone concentration) and the next ant doing so. The real-time value of this computational time step is expected

to decrease for increasing ant populations, since more ants are expected to assess their tasks per unit of real time when the population is large. A given ant assesses its cues on average once every M time steps, where M equals the total number of time steps used in a simulation divided by the total number of ants. In our model, the cue (or 'field') is computed using a fixed fraction of the total ant population.

If the population of category X is large around the time an ant is updating its category, this category X will contribute strongly to the field sampled by this ant. Likewise, if the population of X is large, the encounter rate of the ant with category X ants will be high. The role of encounter rates as well as their regulation as a function of colony density (Gordon *et al.*, 1993) has been under scrutiny recently in the context of foraging efficiency and flexibility (Bonabeau *et al.*, 1998b) and task allocation (Gordon, 1996; Gordon and Mehdiabadi, 1999b). Our model could thus be interpreted as one in which the rate of encounter with ants of different categories is the driving force behind the field assessment. Our time step could then be interpreted as the mean time interval required to estimate 'a rate of contact', and thus to decide whether or not to switch categories. It would be worthwhile to further investigate the behavior of recovery time with increasing N under various assumptions [e.g., as in Pacala *et al.* (1996)], with and without external stimuli.

However, our model does not keep track of the fluctuations in, e.g., category X during the whole time interval (M time steps) between two successive updates of the same ant. Rather, the updating is done based on current population numbers at the time of updating. This could nevertheless provide a reasonable estimate of encounter rate if fluctuations in population numbers are slow, which may or may not be the case depending on model parameters. As our birth–death formalism allows the calculation of such fluctuation properties, we could determine the conditions where fluctuations on stochastic attractors are slow; this will be left for future work. A more accurate estimation of contact rate, in a more sophisticated version of our threshold model (or of the eight-category model of Gordon *et al.*, 1992) could be done, for example, by using field values that are weighted averages over population numbers during some recent time window.

6.3.3. *Other avenues of interest.* It would also be of interest to include spatial segregation of tasks, e.g., as in Solé *et al.* (1993). In the birth–death representation, the model would become equivalent to a spatially extended nonlinear chemical system (see the end of Section 4 for an analogy of our model with chemical reactions). One could also study how task allocation generates and updates the *dynamical rules* determining the distribution into different tasks for each ecological situation. It would be interesting then to examine how natural selection could have acted to provide for an optimal way to switch from one task to another, instead of producing fixed ratios of individuals occupied at various tasks. For example, in an ant colony, there may have been a propensity for an outside worker to switch to foraging when a new food source appeared, rather than selection for higher numbers of foragers (Gordon, 1996, 1999a).

Following this scenario, the interaction matrix can be thought to have changed over the course of evolution. Initially, there may have been no switching between categories, such as if behaviors of the units were preprogrammed in the genetics. Alternately, there may have been, initially, no interactions, but instead a propensity to switch, e.g., randomly or depending on environmental stimuli; this propensity could have been programmed into each unit. Subsequently, interactions within a category may have developed, followed by interactions between categories. Our preliminary investigations of one evolution scenario, starting from an initial 'interactionless' situation, suggests that the evolution of a cross-interaction is 'safe' for a species because it does not alter drastically its own current population dynamics. Only later on, as cross-interactions become as strong as self interactions, would behavior be altered significantly as tighter population control (smaller attractor widths) arises. Our model offers a simple tool for the investigation of such evolution scenarios with and without external stimuli.

Finally, it would certainly be of interest to explore the dynamics of similar models but with higher numbers of categories. This would be directly relevant to the aforementioned studies of task allocation in insects (Bonabeau *et al.*, 1998a; Gordon, 1999a; Beshers and Fewell, 2001). It would be particularly exciting to understand from a dynamical point of view why a given species has a given number of worker categories and what aspects of the global network organization are being optimized by the dynamics.

ACKNOWLEDGEMENTS

We thank Brent Doiron for useful discussions. This research was supported by the Natural Science and Engineering Research Council of Canada.

APPENDIX A

A birth–death process such as the one we used to model task switching is characterized by the conditional probability $P(x, t|x_0, 0)$, where x_0 is the initial population at time t_0 (t_0 is chosen here to be zero). This probability evolves according to the following so-called 'master equation' (Gardiner, 1985):

$$\frac{\partial P(x,t|x_0,0)}{\partial t} = t^+(x-1)P(x-1,t|x_0,0) + t^-(x+1)P(x+1,t|x_0,0) \quad \text{(A1)}$$

$$-(t^+(x) + t^-(x))P(x,t|x_0,0). \quad \text{(A2)}$$

Here, $t^+(x)$ is the transition probability per unit time of a forward transition $x \to x+1$, while $t^-(x)$ is the transition probability per unit time of a backward transition $x \to x-1$. The first term on the right-hand side accounts for the

increase of $P(x,t)$ due to forward transitions from the state $x-1$, while the second accounts for the increase of $P(x,t)$ due to backward transitions from the state $x+1$. The last two terms account for decreases in $P(x,t)$ due to, respectively, forward and backward transitions from the state x.

Confining our analysis to the trapping region in Fig. 7 (or Fig. 5), we have the aforementioned transition probabilities $t^+(x) = 1 - \frac{x}{N}$ and $t^-(x) = x/N$, which are, respectively, the probabilities of choosing the CAT 2 map and the CAT 1 map shown in Fig. 9. Since we are in the trapping region, we also have $t^-(n_a) = t^+(n_b) = 0$, and the steady-state probabilities $P_s(x) = 0$ for $0 \leq x \leq n_a - 1$ or $(n_b + 1 \leq x \leq N)$.

It is possible to solve the master equation analytically for the steady-state probability $P_s(x)$ (we omit the conditional notation for clarity). In terms of the probability current $J(x)$

$$J(x) = t^-(x)P_s(x) - t^+(x-1)P_s(x-1) \tag{A3}$$

the steady-state condition can be written as

$$0 = J(x+1) - J(x). \tag{A4}$$

Summing this equation from $x = n_a$ to $x-1$ leads to:

$$0 = \sum_{z=n_a}^{x-1} [J(x+1) - J(x)] = J(x) - J(n_a). \tag{A5}$$

Thus, the steady-state condition is $J(x) = J(n_a)$, i.e., $J(x) = 0$ by the boundary conditions previously given. This implies that

$$P_s(x) = \frac{t^+(x-1)}{t^-(x)} P_s(x-1) \tag{A6}$$

and hence, that

$$P_s(x) = \frac{t^+(x-1)t^+(x-2)\ldots t^+(n_a)}{t^-(x)t^-(x-1)\ldots t^-(n_a+1)} P_s(n_a). \tag{A7}$$

This probability depends on the number $P_s(n_a)$, which in practice can be factored into a normalization factor for the probability density, yielding the normalized density:

$$P_s(x) = \frac{\prod_{x=n_a+1}^{x} \frac{t^+(x-1)}{t^-(x)}}{\sum_{n_a+1}^{n_b} \prod_{x=n_a+1}^{n_b} \frac{t^+(x-1)}{t^-(x)}}. \tag{A8}$$

Further simplification of this expression is possible by writing in the expressions for $t^+(x)$ and $t^-(x)$ and by introducing binomial coefficients. It is straightforward

to show that the numerator is in fact given by the binomial coefficient $\binom{N}{x}$ divided by $\binom{N}{n_a}$. The asymptotic density can thus be written more simply as:

$$P_s(x) = \frac{\binom{N}{x}}{\sum_{x=n_a+1}^{n_b} \binom{N}{x}}. \tag{A9}$$

The birth–death master equation formalism also allows us to compute the evolution of moments of these distributions and of correlation functions of the state variable. For example, in the presence of fluctuations, the mean evolves according to:

$$\frac{d}{dt}\langle x(t)\rangle = \langle t^+[x(t)]\rangle - \langle t^-[x(t)]\rangle, \tag{A10}$$

where the brackets denote ensemble averages over the different possible paths of this stochastic process. The corresponding deterministic equation is $dx/dt = t^+(x) - t^-(x)$. In the steady state, the mean is then simply given by the solution of $t^+(x^*) = t^-(x^*)$, i.e., $x^* = N/2$ for the example given previously. Intuitively, the dynamics are similar to the stochastic overdamped motion of a particle in a parabolic potential $U(x)$ (the negative gradient of which equals $d\langle x(t)\rangle/dt$); this motion is constrained by the reflecting boundaries of the trapping region.

REFERENCES

Barnsley, M. F. and S. G. Demko (1985). Iterated function systems and the global construction of fractals. *Proc. Roy. Soc. London Sec. A* **399**, 243–275.

Beshers, S. N. and J. H. Fewell (2001). Models of division of labor in social insects. *Annu. Rev. Entomol.* **46**, 413–440.

Bonabeau, E., G. Theraulaz, J. L. Deneubourg, S. Aron and S. Camazine (1997). Self-organization in social insects. *Trends Ecol. Evol.* **12**, 188–193.

Bonabeau, E., G. Theraulaz and J. L. Deneubourg (1998a). Fixed response thresholds and the regulation of division of labor in insect societies. *Bull. Math. Biol.* **60**, 753–807.

Bonabeau, E., G. Theraulaz and J. L. Deneubourg (1998b). Group and mass recruitment in ant colonies: the influence of contact rates. *J. Theor. Biol.* **195**, 157–166.

Borkar, V. S., S. Jain and G. Rangarajan (1998). Dynamics of individual specialization and global diversification in communities. *Complexity* **3**, 50–56.

Delgado, J. and R. V. Solé (1998). Mean-field theory of fluid neural networks. *Phys. Rev. E.* **57**, 2204–2211.

Deneubourg, J. L., S. Aron, S. Goss, J. M. Pasteels and G. Duerinck (1986). Random behavior, amplification processes and number of participants: how they contribute to the foraging properties of ants. *Physica D* **22**, 176–186.

Deneubourg, J. L. and N. R. Franks (1995). Collective control without explicit coding: The case of communal nest excavation. *J. Insect Behav.* **8**, 417–432.

Gardiner, C. W. (1985). *Handbook of Stochastic Methods for Physics, Chemistry and the Natural Sciences*, Berlin: Springer-Verlag.

Gordon, D. M., B. C. Goodwin and L. E. H. Trainor (1992). A parallel distributed model of the behavior of ant colonies. *J. Theor. Biol.* **156**, 293–307.

Gordon, D. M., R. E. Paul and K. Thorpe (1993). What is the function of encounter patterns in ant colonies? *Anim. Behav.* **45**, 1083–1100.

Gordon, D. M. (1996). The organization of work in social insect colonies. *Nature* **380**, 121–124.

Gordon, D. M. (1999a). *Ants at Work: How an Insect Society is Organized*, New York: The Free Press.

Gordon, D. M. and N. J. Mehdiabadi (1999b). Encounter rate and task allocation in harvester ants. *Behav. Ecol. Sociobiol.* **45**, 370–377.

Hertz, J., A. Krogh and R. G. Palmer (1991). *Introduction to the Theory of Neural Computation*, Vol. I, Santa Fe Institute Studies in the Sciences of Complexity, Reading, MA: Addison and Wesley.

Hofbauer, J. and K. Sigmund (1991). *The Theory of Evolution and Dynamical Systems*, Vol. 7, London Math. Soc. Student Texts, Cambridge: Cambridge University Press.

Hopfield, J. J. K. (1982). Neural networks and physical systems with emergent collective computational abilities. *Proc. Natl. Acad. Sci. USA* **79**, 2554–2558.

Kauffman, S. A. (1990). Requirements for evolvability in complex systems: orderly dynamics and frozen components. *Physica D* **42**, 135–152.

Lewis, J. E. and L. Glass (1992). Nonlinear dynamics and symbolic dynamics of neural networks. *Neural Comput.* **4**, 621–642.

Pacala, S. W., D. M. Gordon and H. C. Godfray (1996). Effects of social group size on information transfer and task allocation. *Evol. Ecol.* **10**, 127–165.

Page, R. E. and S. D. Mitchell (1990). Self-organization and adaptation in insect societies, in *Phil. Sci. Assoc.*, Vol. 2, A. Fine, M. Forbes and L. Wessels (Eds), East Lansing, MI: Philos. Sci. Assoc., pp. 289–298.

Parrish, J. K. and L. Edelstein-Keshet (1999). Complexity, pattern, and evolutionary trade-offs in animal aggregation. *Science* **284**, 99–101.

Pathria, R. K. (1984). *Statistical Mechanics*, Oxford: Pergamon Press.

Poon, L. and C. Grebogi (1995). Controlling complexity. *Phys. Rev. Lett.* **75**, 4023–4026.

Sendova-Franks, A. B. and N. R. Franks (1995). Spatial relationships within nests of the ant Leptothorax unifaxciatus (Latr.) and their implications for the division of labour. *Anim. Behav.* **50**, 121–136.

Solé, R. V., O. Miramontes and B. C. Goodwin (1993). Oscillations and chaos in ant societies. *J. Theor. Biol.* **161**, 343–357.

Somogyi, R. and C. A. Sniegoski (1996). Modeling the complexity of genetic networks: understanding multigenic and pleiotropic regulation. *Complexity* **1**, 45–63.

Tofts, C. and N. R. Franks (1992). Doing the right thing: ants, honeybees and naked molerats. *Trends Ecol. Evol.* **7**, 346–349.

Torres, J. L. and L. E. H. Trainor (1993). Energy function for a model of ant colonies. *J. Theor. Biol.* **165**, 177–184.

Trainor, L. E. H. (1993). Modelling the behavior of ant colonies as an emergent property of a system of ant-ant interactions, in *Thinking About Biology.* Vol. III, Santa Fe Institute Studies in the Sciences of Complexity, D. Stein and F. J. Varela (Eds), Reading, MA: Addison and Wesley, pp. 1–9.

Trainor, L. E. H., W. A. M. Brandts and J. L. Torres (1997). Category switching—A neural network approach, in *Physical Theory in Biology: Foundations and Explorations,* C. J. Lumsden, W. A. M. Brandts and L. E. H. Trainor (Eds), London: World Scientific Publishing, pp. 365–376.

Received 3 September 2000 and accepted 2 August 2001